THE JOURNAL OF PHYSICAL CHEMISTRY A

Article

pubs.acs.org/JPCA

Photoelectron Spectroscopic and Computational Study of Pyridine-Ligated Gold Cluster Anions

Published as part of The Journal of Physical Chemistry virtual special issue "Veronica Vaida Festschrift".

Gaoxiang Liu, Sandra M. Ciborowski, and Kit H. Bowen*

Department of Chemistry, Johns Hopkins University, 3400 N. Charles Street, Baltimore, Maryland 21218, United States

Supporting Information

ABSTRACT: Pyridine-ligated gold cluster anions were studied through a combination of negative ion photoelectron spectroscopy and density functional theory calculations. Small gold cluster anions ligated by pyridine, $Au_n(py)^-$ were generated with a ligation cell coupled to a laser vaporization source (LVS). We showed that pyridine is weakly bound (physisorbed) to the Au_2^- moiety of $Au_2(py)^-$ by interactions between its gold atoms and either the hydrogen atoms or the π-ring of pyridine. We also found that pyridine's lone electron pair strongly binds (chemisorbs) to both $Au_3(py)^-$ and $Au_4(py)^-$ through single gold atoms on each of these clusters. Bonding analysis of two isomers of $Au_4(py)^-$ supported the presence of two different ligand binding motifs, these differing in terms of the gold atom to which pyridine binds.

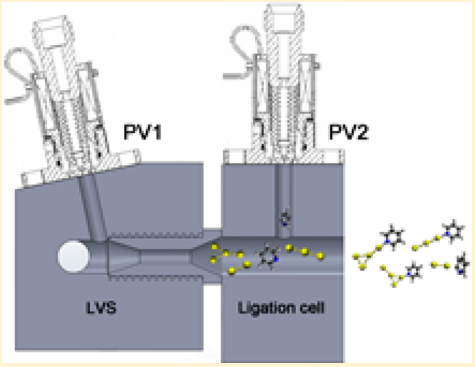

INTRODUCTION

The synthesis of subnanometer gold clusters with a precise number of metal atoms and organic ligands has been the subject of intensive research.[1] The size-dependent physical and chemical properties of these nanoclusters have made them promising materials for a broad range of applications including catalysis,[2−5] chemical sensing,[6,7] optical imaging[8,9] and biomedicine.[10−12] Particular compositions are often achieved by solution-phase reduction syntheses, including size-focusing methodologies[13] or ligand-exchange-induced size/structure transformation processes.[14] Organic ligands such as thiols,[15] phosphines,[16] and alkynes[17] are used to control the growth of gold clusters to specific sizes and to stabilize the prepared nanoclusters.[13] The bonding and interaction between specific organic ligands and gold cluster cores play a critical role in determining the structure, stability, and functionality of gold nanoclusters.[18] Metal−ligand interactions are also relevant to metal−protein recognition at a molecular level, with these guiding the synthesis of metalloproteins having desirable properties.[19]

Extensive theoretical work has investigated the effect of ligation on the structures and energetics of various size gold cluster cores.[20−22] Examining how certain ligands can stabilize gold clusters of specific size has provided insight into the growth mechanism of atomically precise ligated gold clusters.[20−22] For example, density functional theory (DFT) calculations were performed on the absorption of methylthiol onto various gold cores Au_n^Z (n = 1−8, 12, 13, 20; Z = 0, −1, +1).[21] In another study, DFT was employed to analyze the binding energies of small Au_n clusters (n = 1−7, 11) with various lone-pair ligands (L = SH_2, NH_3, PCl_3, PMe_3, etc.).[23] For even-sized gold clusters, it was found that covalent Au_n−L bonds were formed when the ligands' (L) lone pairs interacted with the Au_n moiety's lowest unoccupied molecular orbital (LUMO). For odd-sized gold clusters, the bonding was found to be dominated by the interaction between the ligands' lone pairs and the Au_n core's singly occupied molecular orbital (SOMO).[23] Although many theoretical studies have been conducted on the nature of the bonding interactions between gold cluster cores and their ligands, direct experimental measurements pertaining to those interactions have been limited. Ligated gold clusters are commonly characterized by electrospray ionization mass spectrometry (ESI-MS),[24] X-ray diffraction (XRD),[25] and UV−vis spectroscopy,[26] which yield information on the clusters' sizes, crystal structures, and optical properties, respectively. These, however, provide little insight into the nature of binding between ligands and gold clusters.

Recently, gas-phase experiments which couple ESI-MS with techniques, such as collision-induced dissociation (CID) and surface-induced dissociation (SID), have been used to characterize the ligand−core interactions and binding energies of ligated gold clusters.[27] Johnson, Laskin, and co-workers investigated fragmentation patterns and binding energies of mass-selected triphenylphosphine (TPP) ligated gold cluster cations using ESI-MS-SID and found that the $Au_8(TPP)_6^+$ ion is remarkably stable toward dissociation, likely due to its large ligand binding energy.[28] Their strategy, however, required that ligated gold clusters first be synthesized in solution and then

Received: June 12, 2017
Revised: July 13, 2017
Published: July 17, 2017

DOI: 10.1021/acs.jpca.7b05712
J. Phys. Chem. A 2017, 121, 5817−5822

introduced into the gas phase using ESI. The choices of ligated gold clusters that could be studied in the gas phase by this approach were limited to those that could be synthesized in solution.[29−31] Because most of the ligands used in solution synthesis are thiols and phosphines, only a limited number of interaction motifs between ligands and gold cores have been explored with these methods.[1,27] Thus, an experimental approach that affords an opportunity to investigate interactions between a wider variety of ligands and different size gold clusters may help to sample a broader range of interactions.

In this work, a cluster beam source was used to prepare pyridine-ligated gold cluster anions, $Au_n(pyridine)^-$. This source comprises a laser vaporization source (LVS) and a ligation cell. Pyridine (py) was chosen as a ligand for these experiments because of its simplicity and its binding flexibility; it can interact via its lone pair or its π-ring. Moreover, pyridine-ligated gold clusters are not easily synthesized in solution. The $Au_n(py)^-$ cluster anions formed by this source were identified and mass-selected by mass spectrometry (MS), their excess electrons were photodetached and energy-analyzed by anion photoelectron spectroscopy (PES), and the resulting spectra were analyzed and interpreted through density functional theory (DFT) calculations. This combination of experiment and theory led to insight into the nature of the interactions between the gold cluster cores and their pyridine ligand.

EXPERIMENTAL AND COMPUTATIONAL METHODS

Anion photoelectron spectroscopy is conducted by crossing a beam of mass-selected negative ions with a fixed-frequency photon beam and energy-analyzing the resultant photodetached electrons. The photodetachment process is governed by the energy-conserving relationship $h\nu$ = EBE + EKE, where $h\nu$ is the photon energy, EBE is the electron binding energy, and EKE is the electron kinetic energy. Our apparatus consists of a laser vaporization cluster anion source with an attached ligation cell, a time-of-flight mass spectrometer, a Nd:YAG photodetachment laser, and a magnetic bottle electron energy analyzer.[32] The photoelectron spectrometer resolution is ∼35 meV at 1 eV EKE. The third (355 nm) and fourth (266 nm) harmonic outputs of a Nd:YAG laser were used to photodetach electrons from mass-selected Au_n^- and $Au_n(py)^-$ clusters. Photoelectron spectra were calibrated against the well-known atomic transitions of atomic Cu^-.[33]

A schematic of our LVS-coupled ligation cell source is shown in Figure 1. Gold cluster anions were generated by laser vaporization of a pure gold foil wrapped around an aluminum rod. The resultant plasma was cooled with helium gas delivered by a pulsed valve (PV1) having a backing pressure of a 100 psig. The resulting gold cluster anions then traveled through a ligation cell (4 mm diameter), where they mixed with pyridine vapor. The pyridine vapor was introduced into the ligation cell by a second pulsed valve (PV2). The resulting $Au_n(py)^-$ anionic clusters were mass-analyzed by the time-of-flight mass spectrometer and their photoelectron spectra recorded.

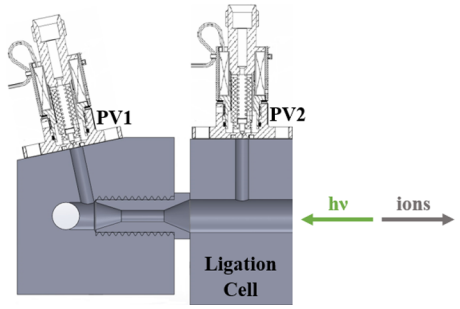

Figure 1. Schematic of the laser vaporization housing coupled with a ligation cell.

Density functional theory calculations were performed with the ORCA computational chemistry software package.[34] All calculations were carried out with the Becke Perdew (BP86) functional[35] with the D3 dispersion correction[36] and the RIJCOSX approximation.[37] The Ahlrichs Def2 basis sets were used throughout our calculations.[38] For geometry optimization, Def2-SVP and auxiliary Def2-SVP/J basis sets were chosen for hydrogen, nitrogen, and carbon atoms; the Stuttgart effective core potential SDD[39] and ECP basis set Def2-TZVP|Def2-TZVP/J were used for gold atoms. Single-point calculations were then improved with larger basis sets: Def2-TZVP|Def2-TZVP/J for hydrogen, nitrogen, and carbon atoms, and SDD|Def2-QZVPP|Def2-QZVPP/J for gold atoms. Vertical detachment energies (VDE) were computed from the energetic difference between the relaxed anionic complex and its corresponding neutral species at the geometry of the relaxed anion. Electron affinities (EA) were calculated from the energy differences between the relaxed anionic complex and its relaxed neutral counterpart. Frequency calculations were performed to verify that no imaginary frequencies existed and all optimized structures were minima.

RESULTS

A. Experimental Section. The mass spectra, with and without pyridine (py) pulsed into the ligation cell, are shown in Figure 2. This work focuses on relatively small gold-pyridine

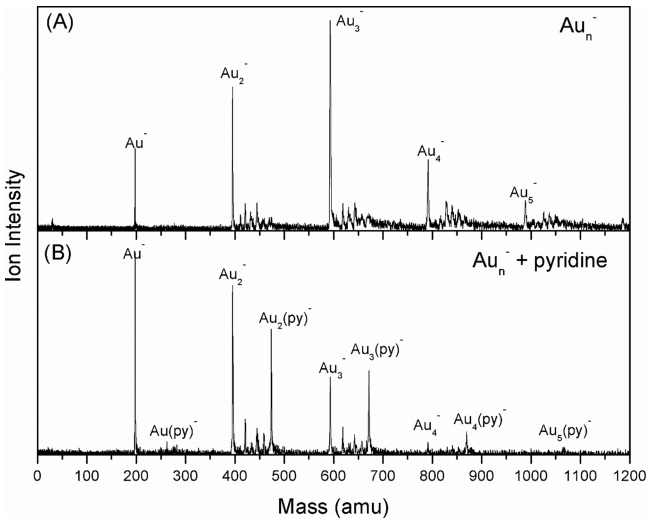

Figure 2. Mass spectra of (A) Au_n^- cluster anions and (B) pyridine-ligated gold cluster anions $Au_n(py)^-$.

clusters. With no pyridine in the ligation cell, Au_n^- cluster anions (n = 2−5) are observed in the mass spectrum; when pyridine is added to the cell, a new series of $Au_n(py)^-$ complexes appears. Though $Au_n(py)^-$ and Au_n^- show comparable ion intensities for n = 2−5, $Au(py)^-$ has a very low ion intensity despite the abundance of Au^-. The mass spectra clearly show that pyridine binds to gold cluster anions.

DOI: 10.1021/acs.jpca.7b05712
J. Phys. Chem. A 2017, 121, 5817−5822

Photoelectron spectra of Au_n^- and $Au_n(py)^-$ were recorded for n = 2−4, and these are displayed in Figure 3. The

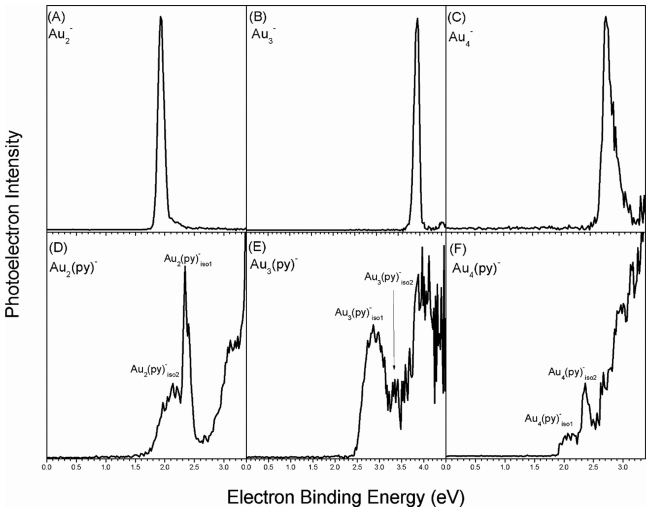

Figure 3. Photoelectron spectra of (A)−(C) Au_n^- and (D)−(F) $Au_n(py)^-$ (n = 2−4).

photoelectron spectra for Au_n^- agree well with those measured in previous studies.[40] For $Au_2(py)^-$, its lowest EBE spectral band covers EBE = 1.7−2.5 eV, and it exhibits two distinct features. These comprise a relatively broad peak centered at EBE = 2.11 eV and a sharp peak centered at EBE = 2.34 eV. These spectral features suggest the coexistence of two $Au_2(py)^-$ isomers, in which their pyridine molecules are weakly bound (physisorbed) to their Au_2^- moieties in both cases. There, the gold dimer anion moieties act as the chromophores for photodetachment, and for that reason the resulting spectra look like Au_2^- spectra, just shifted to slightly higher EBE values by their ion−molecule interaction energies.[41] The electron affinities (EA) for the neutral counterparts of these two isomers, obtained by extrapolating the lower EBE edges of their peaks to baseline, are estimated to be 1.7 and 2.3 eV. (The band at EBE ∼ 3 eV may be due to excited electronic states or to a chemisorbed isomer, but that feature was not pursued in this study.)

For $Au_3(py)^-$ and $Au_4(py)^-$, broad spectral features appear at lower EBE values than those of the relatively narrow peaks of Au_3^- and Au_4^-. This means that they are not weakly bound (physisorbed) anion−molecule complexes. In fact, it implies that the energetics of the molecular orbitals (MO) of the Au_3^- and Au_4^- cores are substantially modified by interaction with pyridine, indicating strong, chemisorbed interactions in these anionic complexes. For $Au_3(py)^-$, transitions with maximum spectral intensities at 2.93 and 3.43 eV are identified, with corresponding EA values of 2.5 and 3.2 eV. For $Au_4(py)^-$, the EBE peaks with maxima at 2.03 and 2.36 eV are likely due to different isomers, and the EA values of their neutral counterparts are determined as 1.9 and 2.2 eV. (The higher EBE features in both of these cases may again be due to excited electronic states or to a chemisorbed isomer, but we did not pursue them in this study.)

B. Computational Details. DFT calculations were performed to account for the multiple features observed in the photoelectron spectra of $Au_n(py)^-$. The optimized structures, relative energies, experimental/theoretical VDE values of $Au_n(py)^-$ and experimental/theoretical EA values of their neutral molecule counterparts, $Au_n(py)$, are presented in Table 1. The lowest energy structure for $Au_2(py)^-$ is a complex

Table 1. Optimized Structures, Relative Energies, Experimental/Theoretical EA Values of Neutral $Au_n(py)$, and Experimental/Theoretical VDE Values of $Au_n(py)^-$ [a]

Anion	Optimized Structure	ΔE	Expt. EA	Theo. EA	Expt. VDE	Theo. VDE
$Au_2(py)^-_{iso1}$	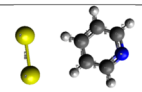	0	2.3	2.36	2.34	2.47
$Au_2(py)^-_{iso2}$	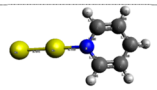	0.06	N/A	0.94	N/A	1.16
$Au_2(py)^-_{iso3}$		0.15	1.7	1.40	2.11	1.96
$Au_3(py)^-_{iso1}$	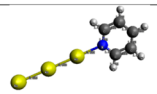	0	2.5	2.68	2.93	2.84
$Au_3(py)^-_{iso2}$	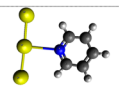	0.19	3.2	2.20	3.43	3.50
$Au_4(py)^-_{iso1}$	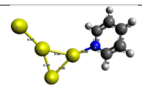	0	1.9	1.41	2.03	1.92
$Au_4(py)^-_{iso2}$	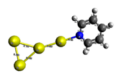	0.18	2.2	2.13	2.36	2.22
$Au_4(py)^-_{iso3}$	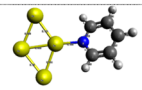	0.21	N/A	1.50	N/A	1.70

[a]The unit of energy is eV. N/A indicates the corresponding isomer was not observed in the experiment.

where the anionic Au_2^- moiety weakly interacts with the hydrogen atoms of pyridine (see $Au_2(py)^-_{iso1}$ in Table 1). The distances between Au and H are around 2.7 Å, which is typical for hydrogen-bond like interaction, i.e., the solvation effect. In $Au_2(py)^-_{iso2}$, the Au_2^- moiety is predicted to interact strongly with pyridine, i.e., a pyridine-ligated Au_2^-, and to exhibit a VDE value of 1.16 eV. There is, however, no feature there in our spectrum. For $Au_2(py)^-_{iso3}$, however, the prediction of a weakly bound complex (VDE = 1.96 eV) is in agreement with the observed feature at VDE = 2.11 eV (see $Au_2(py)^-_{iso3}$ in Table 1). For $Au_3(py)^-$, two stable products were identified. For both isomers, the gold trimer moieties adopted linear geometries. Pyridine ligated the Au_3^- moieties either through the end gold atom (see $Au_3(py)^-_{iso1}$ in Table 1) or through the middle gold atom (see $Au_3(py)^-_{iso2}$). Two of the three calculated $Au_4(py)^-$ cluster anion isomers exhibit corresponding features in the $Au_4(py)^-$ spectrum, and both of these are chemisorbed systems, i.e., pyridine-ligated gold clusters. The Au_4 moieties in $Au_4(py)^-_{iso1}$ and in $Au_4(py)^-_{iso2}$ exhibit Y-shaped structures. There is no evidence for $Au_4(py)^-_{iso3}$ in the photoelectron spectrum; its Au_4 moiety is predicted to have a diamond-shape.

DISCUSSION

Table 1 presents comparisons between experimentally determined and theoretically calculated VDE and EA values. Experimental VDE values are generally more reliable measure-

DOI: 10.1021/acs.jpca.7b05712
J. Phys. Chem. A 2017, 121, 5817−5822

ments than experimental EA values, because the former are simply peak locations, whereas the latter involve extrapolations. Due to differences in the structures of anions and their neutral counterparts, the EA-determining origin transition may not always correspond to the extrapolated lowest EBE side of the spectral band. Table 1 shows excellent agreement between experimental and theoretical VDE values is observed, although for the reasons stated the agreement between experimental and theoretical EA values is not as good.

To understand why the $Au(py)^-$ ion intensity in the mass spectrum is so weak, we calculated the potential energy between a gold anion, Au^-, and a pyridine molecule. As shown in Figure S2, the interaction is largely repulsive. As described above, both the broad peak at EBE = 2.11 eV and the sharp peak at EBE = 2.34 eV in the $Au_2(py)^-$ spectrum are due to weakly bound complexes, where pyridine is physisorbed to the Au_2^- moiety. These VDE values agree relatively well with the calculated VDE values. Moreover, the calculated structures for these isomers are consistent with this interpretation. Because no spectral feature was seen in the vicinity of EBE = 1.16 eV in the photoelectron spectrum, the predicted strongly ligated (chemisorbed) isomer, $Au_2(py)^-_{iso2}$ was not present in the experiment. Its absence may be explained by examining the relaxed potential energy scan shown in Figure S3. There, one sees a 0.62 eV high barrier between $Au_2(py)^-_{iso2}$ and the "weakly-ligated" $Au_2(py)^-_{iso3}$. This barrier may keep $Au_2(py)^-_{iso3}$ from converting to $Au_2(py)^-_{iso2}$, even though the latter is lower in energy. Physically, the barrier is understandable in terms of electrostatic repulsion, i.e., the interaction between pyridine's lone pair and the negatively charged Au_2^- moiety.

The two isomers of the $Au_3(py)^-$ cluster are due to pyridine being chemisorbed (strongly bound) to its gold trimer moiety. The two EBE peaks exhibited in the photoelectron spectrum of $Au_3(py)^-$ correspond to the calculated VDE values of EBE = 2.84 eV and EBE = 3.50 eV. The gold tetramer moieties in $Au_4(py)^-_{iso1}$ and $Au_4(py)^-_{iso2}$ are Y-shaped, and both isomers are chemisorbed (ligated) clusters. The two EBE peaks exhibited in the photoelectron spectrum of $Au_4(py)^-$ correspond to the calculated VDE values of EBE = 1.92 eV and EBE = 2.22 eV. Because no spectral feature was seen in the vicinity of EBE = 1.70 eV in the photoelectron spectrum of $Au_4(py)^-$, the predicted chemisorbed isomer, $Au_4(py)^-_{iso3}$, with its diamond-shaped gold tetramer moiety was not present in the experiment.

The differing bonding motifs in $Au_{1,2}(py)^-$ versus $Au_{3,4}(py)^-$ may be due to different negative charge densities on $Au_{1,2}^-$ versus $Au_{3,4}^-$. Although the excess negative charge is highly localized in the cases of $Au_{1,2}^-$, it is likely to be somewhat delocalized in the cases of $Au_{3,4}^-$. Diffuse electron distributions may have the effect of reducing electrostatic repulsion between $Au_{3,4}^-$ and pyridine and with it the type of barrier seen in Figure S3, making it easier to form chemisorbed (ligated) cluster anions.

To gain more insight into the interaction between pyridine and gold cluster anions, the two isomers of $Au_4(py)^-$ observed in the experiment were selected as candidates for molecular orbital (MO) and charge analyses. The frontier orbitals of $Au_4(py)^-_{iso1}$, $Au_4(py)^-_{iso2}$ and pyridine are presented in Chart 1. The Au_4 moieties in $Au_4(py)^-_{iso1}$ and $Au_4(py)^-_{iso2}$ have net charges of −0.87e and −1.07e, respectively. Orbital analysis indicates that the bonding motif differs depending on which gold atom interacts with pyridine. For $Au_4(py)^-_{iso1}$, though its

Chart 1. Frontier Molecular Orbitals of Pyridine and $Au_4(py)^-$ Cluster Anions Observed in Experiments

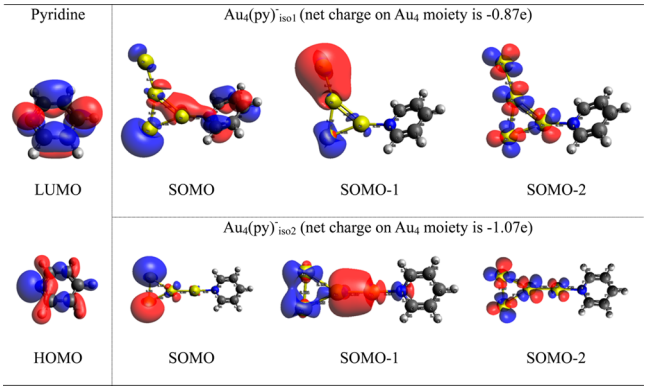

SOMO−1 and SOMO−2 are mostly the MOs of Au_4, its SOMO shows a strong participation of the LUMO of pyridine. The SOMO likely includes strong electron back-bonding from the Au_4 metal core to pyridine. The back-bonding is also manifested by a decrease of the negative charge on Au_4 moiety from −1e to −0.87e. Such back-bonding effects strengthen the interactions between pyridine and the gold cluster, resulting in a shorter, 2.13 Å Au−N bond, compared to the 2.26 Å bond in $Au_4(py)^-_{iso2}$ (Figure S1). The back-bonding also helps to stabilize the anionic complex, making $Au_4(py)^-_{iso1}$ 0.18 eV lower in energy than $Au_4(py)^-_{iso2}$ (Table 1). For $Au_4(py)^-_{iso2}$, its SOMO is mainly the combination of gold atomic orbitals; thus, electron detachment from this orbital should resemble electron detachment from Au_4^-. This is consistent with the sharp transition in the photoelectron spectrum (Figure 3F). The SOMO−1 for $Au_4(py)^-_{iso2}$ shows that the ligand−metal interaction is primarily between the metal core and the lone pair of pyridine.

To summarize this work, a source that couples LVS and a ligation cell was used to make pyridine-ligated gold cluster anions, $Au_n(py)^-$. A combined anion photoelectron spectroscopic and DFT study confirmed the structures of stable $Au_n(py)^-$ (n = 2−4) and explored the nature of their bonding interactions. The excess electrons on the gold cores had significant effects on the structures of the ligated gold cluster anions and thus on their binding motifs.

■ ASSOCIATED CONTENT

Supporting Information

The Supporting Information is available free of charge on the ACS Publications website at DOI: 10.1021/acs.jpca.7b05712.

Optimized structures of $Au_n(py)^-$ and their corresponding neutrals, the potential energy surfaces of $Au(py)^-$ and $Au_2(py)^-$ (PDF)

■ AUTHOR INFORMATION

Corresponding Author

*K. H. Bowen. E-mail: kbowen@jhu.edu.

ORCID

Sandra M. Ciborowski: 0000-0001-9453-4764

Kit H. Bowen: 0000-0002-2858-6352

Notes

The authors declare no competing financial interest.

DOI: 10.1021/acs.jpca.7b05712
J. Phys. Chem. A 2017, 121, 5817−5822

■ ACKNOWLEDGMENTS

This material is based on work supported by the Office of Naval Research (ONR), Multidisciplinary University Research Initiative (MURI) under Grant No. N00014-15-1-2681.

■ REFERENCES

(1) Jin, R.; Zeng, C.; Zhou, M.; Chen, Y. Atomically Precise Colloidal Metal Nanoclusters and Nanoparticles: Fundamentals and Opportunities. *Chem. Rev.* **2016**, *116*, 10346−10413.
(2) Zhu, Y.; Qian, H.; Zhu, M.; Jin, R. Thiolate-Protected Au_n Nanoclusters as Catalysts for Selective Oxidation and Hydrogenation Processes. *Adv. Mater.* **2010**, *22*, 1915−1920.
(3) Gaur, S.; Wu, H.; Stanley, G. G.; More, K.; Kumar, C. S. S. R.; Spivey, J. J. CO Oxidation Studies over Cluster-Derived Au/TiO_2 and AUROlite Au/TiO_2 Catalysts using DRIFTS. *Catal. Today* **2013**, *208*, 72−81.
(4) Chen, W.; Chen, S. Oxygen Electroreduction Catalyzed by Gold Nanoclusters: Strong Core Size Effects. *Angew. Chem., Int. Ed.* **2009**, *48*, 4386−4389.
(5) Yu, C.; Li, G.; Kumar, S.; Kawasaki, H.; Jin, R. Stable $Au_{25}(SR)_{18}/TiO_2$ Composite Nanostructure with Enhanced Visible Light Photocatalytic Activity. *J. Phys. Chem. Lett.* **2013**, *4*, 2847−2852. Oliver-Meseguer, J.; Cabrero-Antonino, J. R.; Domínguez, I.; Leyva-Pérez, A.; Corma, A. Small Gold Clusters Formed in Solution Give Reaction Turnover Numbers of 10^7 at Room Temperature. *Science* **2012**, *338*, 1452−1455.
(6) Muhammed, M. A. H.; Verma, P. K.; Pal, S. K.; Kumar, R. C. A.; Paul, S.; Omkumar, R. V.; Pradeep, T. Bright, NIR-Emitting Au_{23} from Au_{25}: Characterization and Applications Including Biolabeling. *Chem. - Eur. J.* **2009**, *15*, 10110−10120.
(7) Wu, Z.; Wang, M.; Yang, J.; Zheng, X.; Cai, W.; Meng, G.; Qian, H.; Wang, H.; Jin, R. Fluorescent Probes: Well-Defined Nanoclusters as Fluorescent Nanosensors: A Case Study on $Au_{25}(SG)_{18}$ (Small 13/2012). *Small* **2012**, *8*, 2027.
(8) Ramakrishna, G.; Varnavski, O.; Kim, J.; Lee, D.; Goodson, T. Quantum-Sized Gold Clusters as Efficient Two-Photon Absorbers. *J. Am. Chem. Soc.* **2008**, *130*, 5032−5033.
(9) Philip, R.; Chantharasupawong, P.; Qian, H.; Jin, R.; Thomas, J. Evolution of Nonlinear Optical Properties: From Gold Atomic Clusters to Plasmonic Nanocrystals. *Nano Lett.* **2012**, *12*, 4661−4667.
(10) George, A.; Shibu, E. S.; Maliyekkal, S. M.; Bootharaju, M. S.; Pradeep, T. Luminescent, Freestanding Composite Films of Au_{15} for Specific Metal Ion Sensing. *ACS Appl. Mater. Interfaces* **2012**, *4*, 639−644.
(11) Tan, X.; Jin, R. Ultrasmall Metal Nanoclusters for Bio-Related Applications. *WIREs Nanomed. Nanobiotechnol.* **2013**, *5*, 569−581.
(12) Wong, O. A.; Hansen, R. J.; Ni, T. W.; Heinecke, C. L.; Compel, W. S.; Gustafson, D. L.; Ackerson, C. J. Structure-Activity Relationships for Biodistribution, Pharmacokinetics, and Excretion of Atomically Precise Nanoclusters in a Murine Model. *Nanoscale* **2013**, *5*, 10525−10533.
(13) Jin, R.; Qian, H.; Wu, Z.; Zhu, Y.; Zhu, M.; Mohanty, A.; Garg, N. Size Focusing: A Methodology for Synthesizing Atomically Precise Gold Nanoclusters. *J. Phys. Chem. Lett.* **2010**, *1*, 2903−2910.
(14) Zeng, C.; Chen, Y.; Das, A.; Jin, R. Transformation Chemistry of Gold Nanoclusters: From One Stable Size to Another. *J. Phys. Chem. Lett.* **2015**, *6*, 2976−2986.
(15) Negishi, Y.; Nobusada, K.; Tsukuda, T. Glutathione-Protected Gold Clusters Revisited: Bridging the Gap between Gold(I)-Thiolate Complexes and Thiolate-Protected Gold Nanocrystals. *J. Am. Chem. Soc.* **2005**, *127*, 5261−5270.
(16) Wan, X.-K.; Lin, Z.-W.; Wang, Q.-M. Au_{20} Nanocluster Protected by Hemilabile Phosphines. *J. Am. Chem. Soc.* **2012**, *134*, 14750−14752.
(17) Maity, P.; Tsunoyama, H.; Yamauchi, M.; Xie, S.; Tsukuda, T. Organogold Clusters Protected by Phenylacetylene. *J. Am. Chem. Soc.* **2011**, *133*, 20123−20125.
(18) Walter, M.; Akola, J.; Lopez-Acevedo, O.; Jadzinsky, P. D.; Calero, G.; Ackerson, C. J.; Whetten, R. L.; Grönbeck, H.; Häkkinen, A. Unified View of Ligand-Protected Gold Clusters as Superatom Complexes. *Proc. Natl. Acad. Sci. U. S. A.* **2008**, *105*, 9157−9162.
(19) Dudev, T.; Lim, C. Metal Binding Affinity and Selectivity in Metalloproteins: Insights from Computational Studies. *Annu. Rev. Biophys.* **2008**, *37*, 97−116.
(20) Shafai, G.; Hong, S.; Bertino, M.; Rahman, T. S. Effect of Ligands on the Geometric and Electronic Structure of Au_{13} Clusters. *J. Phys. Chem. C* **2009**, *113*, 12072−12078.
(21) Barngrover, B. M.; Aikens, C. M. Oxidation of Gold Clusters by Thiols. *J. Phys. Chem. A* **2013**, *117*, 5377−5384.
(22) Jiang, D. The Expanding Universe of Thiolated Gold Nanoclusters and Beyond. *Nanoscale* **2013**, *5*, 7149−7160.
(23) Rajský, T.; Urban, M. Au_n (n = 1, 11) Clusters Interacting with Lone-Pair Ligands. *J. Phys. Chem. A* **2016**, *120*, 3938−3949.
(24) Black, D. M.; Bhattarai, N.; Whetten, R. L.; Bach, S. B. H. Collision-Induced Dissociation of Monolayer Protected Clusters Au_{144} and Au_{130} in an Electrospray Time-of-Flight Mass Spectrometer. *J. Phys. Chem. A* **2014**, *118*, 10679−10687.
(25) Crasto, D.; Malola, S.; Brosofsky, G.; Dass, A.; Häkkinen, H. Single Crystal XRD Structure and Theoretical Analysis of the Chiral $Au_{30}S(S\text{-}t\text{-}Bu)_{18}$ Cluster. *J. Am. Chem. Soc.* **2014**, *136*, 5000−5005.
(26) Zeng, C.; Liu, C.; Pei, Y.; Jin, R. Thiol Ligand-Induced Transformation of $Au_{38}(SC_2H_4Ph)_{24}$ to $Au_{36}(SPh\text{-}t\text{-}Bu)_{24}$. *ACS Nano* **2013**, *7*, 6138−6145.
(27) Johnson, G. E.; Laskin, J. Understanding Ligand Effects in Gold Clusters using Mass Spectrometry. *Analyst* **2016**, *141*, 3573−3589.
(28) Johnson, G. E.; Priest, T.; Laskin, J. Size-Dependent Stability toward Dissociation and Ligand Binding Energies of Phosphine Ligated Gold Cluster Ions. *Chem. Sci.* **2014**, *5*, 3275−3286.
(29) Johnson, G. E.; Olivares, A.; Hill, D.; Laskin, J. Cationic Gold Clusters Ligated with Differently Substituted Phosphines: Effect of Substitution on Ligand Reactivity and Binding. *Phys. Chem. Chem. Phys.* **2015**, *17*, 14636−14646.
(30) Johnson, G. E.; Priest, T.; Laskin, J. Synthesis and Characterization of Gold Clusters Ligated with 1,3-Bis(dicyclohexylphophino)-propane. *ChemPlusChem* **2013**, *78*, 1033−1039.
(31) Chakraborty, P.; Baksi, A.; Khatun, E.; Nag, A.; Ghosh, A.; Pradeep, T. Dissociation of Gas Phase Ions of Atomically Precise Silver Clusters Reflects Their Solution Phase Stability. *J. Phys. Chem. C* **2017**, *121*, 10971−10981.
(32) Zhang, X.; Liu, G.; Ganteför, G.; Bowen, K. H.; Alexandrova, A. N. $PtZnH_5^-$, A σ-Aromatic Cluster. *J. Phys. Chem. Lett.* **2014**, *5*, 1596−1601.
(33) Ho, J.; Ervin, K. M.; Lineberger, W. C. Photoelectron Spectroscopy of Metal Cluster Anions: Cu_n^-, Ag_n^-, and Au_n^-. *J. Chem. Phys.* **1990**, *93*, 6987−7002.
(34) Neese, F. The ORCA Program System. *WIREs Comput. Mol. Sci.* **2012**, *2*, 73−78.
(35) Becke, A. D. Density-Functional Exchange-Energy Approximation with Correct Asymptotic Behavior. *Phys. Rev. A: At., Mol., Opt. Phys.* **1988**, *38*, 3098−3100. Perdew, J. P. Density-Functional Approximation for the Correlation Energy of the Inhomogeneous Electron Gas. *Phys. Rev. B: Condens. Matter Mater. Phys.* **1986**, *33*, 8822−8824.
(36) Grimme, S.; Antony, J.; Ehrlich, S.; Krieg, H. A Consistent and Accurate *Ab Initio* Parametrization of Density Functional Dispersion Correction (DFT-D) for the 94 Elements H-Pu. *J. Chem. Phys.* **2010**, *132*, 154104.
(37) Neese, F.; Wennmohs, F.; Hansen, A.; Becker, U. Efficient, Approximate and Parallel Hartree-Fock and Hybrid DFT Calculations. A 'Chain-of-Spheres' Algorithm for the Hartree-Fock Exchange. *Chem. Phys.* **2009**, *356*, 98−109.
(38) Weigend, F.; Ahlrichs, R. Balanced Basis Sets of Split Valence, Triple Zeta Valence and Quadruple Zeta Valence Quality for H to Rn: Design and Assessment of Accuracy. *Phys. Chem. Chem. Phys.* **2005**, *7*, 3297−3305. Weigend, F. Accurate Coulomb-Fitting Basis Sets for H to Rn. *Phys. Chem. Chem. Phys.* **2006**, *8*, 1057−1065.

DOI: 10.1021/acs.jpca.7b05712
J. Phys. Chem. A 2017, 121, 5817−5822

(39) Andrae, D.; Häußermann, U.; Dolg, M.; Stoll, H.; Preuß, H. Energy-Adjusted *Ab Initio* Pseudopotentials for the Second and Third Row Transition Elements. *Theor. Chim. Acta* **1990**, *77*, 123−141.
(40) Häkkinen, H.; Yoon, B.; Landman, U.; Li, X.; Zhai, H.-J.; Wang, L.-S. On the Electronic and Atomic Structures of Small Au_N^- (N = 4−14) Clusters: A Photoelectron Spectroscopy and Density-Functional Study. *J. Phys. Chem. A* **2003**, *107*, 6168−6175.
(41) Zhang, X.; Lim, E.; Kim, S. K.; Bowen, K. H. Photoelectron Spectroscopic and Computational Study of $(M\text{-}CO_2)^-$ Anions, M = Cu, Ag, Au. *J. Chem. Phys.* **2015**, *143*, 174305.

DOI: 10.1021/acs.jpca.7b05712
J. Phys. Chem. A 2017, 121, 5817−5822